

# High-pressure single-crystal neutron scattering study of magnetic and Fe vacancy orders in $(\text{Tl,Rb})_2\text{Fe}_4\text{Se}_5$ superconductor

Feng Ye,<sup>1,2</sup> Wei Bao,<sup>3,\*</sup> Songxue Chi,<sup>1</sup> Antonio M. dos Santos,<sup>1</sup> Jamie J. Molaison,<sup>1</sup> Minghu Fang,<sup>4</sup> Hangdong Wang,<sup>4</sup> Qianhui Mao,<sup>4</sup> Jinchen Wang,<sup>3</sup> Juanjuan Liu,<sup>3</sup> and Jieming Sheng<sup>3</sup>

<sup>1</sup>Quantum Condensed Matter Division, Oak Ridge National Laboratory, Oak Ridge, Tennessee 37831, USA

<sup>2</sup>Department of Physics and Astronomy, University of Kentucky, Lexington, Kentucky 40506, USA

<sup>3</sup>Department of Physics, Renmin University of China, Beijing 100872, China

<sup>4</sup>Department of Physics, Zhejiang University, Hangzhou 310027, China

The magnetic and iron vacancy orders in superconducting  $(\text{Tl,Rb})_2\text{Fe}_4\text{Se}_5$  single-crystals were investigated using a high-pressure neutron diffraction technique. Similar to the temperature effect, the block antiferromagnetic order gradually decreases upon increasing pressure while the Fe vacancy superstructural order remains intact before its precipitous disappearance at the critical pressure  $P_c = 8.3$  GPa. Combined with previously determined  $P_c$  for superconductivity, our phase diagram under pressure reveals the concurrence of the block AFM order, the  $\sqrt{5} \times \sqrt{5}$  iron vacancy order and superconductivity for the 245 superconductor. A synthesis of current experimental data in a coherent physical picture is attempted.

PACS numbers: 74.62.Fj, 25.40.Dn, 74.25.Ha, 74.70.-b

The recently discovered metal-intercalated iron selenide superconductors  $A_2\text{Fe}_4\text{Se}_5$  ( $A=\text{K}, \text{Cs}, \text{Tl-K}, \text{Rb}, \text{Tl-Rb}$ ) (245) compounds, with  $T_c \sim 30$  K, have attracted much interest [1, 2]. A high transition-temperature ( $T_N \approx 470\text{-}560$  K) and large magnetic moment ( $3.3\mu_B/\text{Fe}$ ) block antiferromagnetic (AFM) order exists in the superconducting samples [3–5]. And magnetic order-parameter experiences an anomaly when  $T_c$  is approached [4, 5]. The superconductors crystallize with a highly ordered  $\sqrt{5} \times \sqrt{5}$  superstructure, in which the Fe1 site of the  $I4/m$  structure is only a few percent occupied and the Fe2 site fully occupied [4, 6]. The non-superconducting samples at low- $T$  also crystallize in the  $I4/m$  structure, but both Fe sites are *fractionally* occupied [7, 8], since the numbers of the Fe vacancies in the samples and the vacant sites in the  $\sqrt{5} \times \sqrt{5}$  pattern are mismatched. The partially ordered  $\sqrt{5} \times \sqrt{5}$  vacancy order becomes one of three competing phases for temperature below the room temperature up to  $\sim 500$  K, namely, these samples are phase-separated and in the miscibility gap at ambient condition [8, 9].

Close to the miscibility gap, it is not surprising that the nonstoichiometric 245 superconductors often contain several phases of different space-group symmetry. It has been a complex and controversial issue to determine the sample composition of the superconductors. The  $\text{KFe}_{1.5}\text{Se}_2$  (234) of the orthorhombic Fe vacancy order has been proposed as the parent compound [10]. However, this phase is not even the ground state for  $\text{KFe}_{1.5}\text{Se}_2$ , and a partially ordered  $\sqrt{5} \times \sqrt{5}$  vacancy superlattice is more stable at low temperature [8]. The  $\text{KFe}_2\text{Se}_2$  (122) of  $I4/mmm$  symmetry has also been proposed as the superconducting phase [11]. But its existence in films grown by molecular beam epitaxy method likely requires charge transfer with the substrate, and there is no trace of its existence in bulk superconduct-

ing samples [4, 12]. Detected in the 245 superconductors is the alkaline metal deficient  $A_x\text{Fe}_2\text{Se}_2$  ( $x \sim 0.3\text{-}0.6$ ) phase embedded in  $\sqrt{5} \times \sqrt{5}$  iron vacancy ordered superstructure [12–14], forming various microstructure patterns in plane [15, 16] or heterostructure along the  $c$ -axis [9, 13, 17] depending on sample preparation procedures. The average sample compositions of these superconductors are consistent with the phase diagram in [8]. The question is what role the  $A_x\text{Fe}_2\text{Se}_2$  ( $x \sim 0.3\text{-}0.6$ ), the  $\sqrt{5} \times \sqrt{5}$  superstructure and the AFM order play in the 245 superconductors.

High pressure adds an additional dimension to the complex composition phase-diagram of 245 superconductors [8], offering a “clean” way to investigate the relation among various phases [18, 19]. The  $T_c$  has been suppressed to zero at critical pressure  $P_c \approx 6$  GPa for  $A=\text{Rb}$  [19, 20], 8 GPa for  $A=\text{Cs}$  [21], and 9 GPa for  $A=\text{K}$  and  $\text{Tl-Rb}$  superconductors [22]. In the latter study, superconductivity of a higher  $T_c = 48$  K is reported to re-emerge between 11 and 13 GPa [22]. High-pressure x-ray powder diffraction experiments have been performed at room temperature, but differing results have been reported: the  $I4/m$  phase is replaced by an  $I4/mmm$  phase at  $P_c$  in one study [18], but the  $I4/m$  phase remains up to 15.6 GPa well above  $P_c$  in the other [20]. In a high-pressure Mössbauer spectroscopic study, it has been concluded that the  $A_x\text{Fe}_2\text{Se}_2$  phase in the sample remains intact up to 13.8 GPa. What has changed is the AFM order on the  $\sqrt{5} \times \sqrt{5}$  superstructure which is *partially* replaced by a new paramagnetic phase after the superconductivity is suppressed at the critical pressure  $P_c$  [20]. Therefore, no clear relationship has been established between the superconductivity and either the  $A_x\text{Fe}_2\text{Se}_2$  phase, the  $\sqrt{5} \times \sqrt{5}$  superstructure, or the AFM order in current high pressure studies.

Here we report high-pressure single-crystal neutron

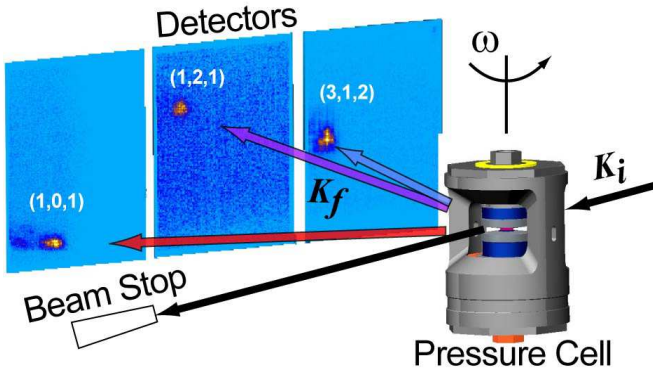


FIG. 1. (color online) Schematic diagram of the single-crystal neutron diffraction experiments at SNAP. The semi-white neutron beam reaches the sample inside the anvil cell and is diffracted into the position sensitive detectors.

diffraction study of the  $(\text{Tl,Rb})_2\text{Fe}_4\text{Se}_5$  superconductor up to 9 GPa, measuring simultaneously the AFM order and the crystal structure. The  $\sqrt{5} \times \sqrt{5}$  vacancy order persists under pressure until its precipitous destruction near  $P_c \approx 8.3$  GPa when the AFM order parameter is reduced progressively to zero. The disappearance of the magnetic and structural orders coincides with the suppression of superconductivity, revealing the importance of the block AFM order and the  $I4/m$  vacancy order in stabilizing superconductivity in the 245 superconductor.

Single crystals of  $(\text{Tl,Rb})_2\text{Fe}_4\text{Se}_5$  ( $T_c \approx 32.5$  K) were grown using the Bridgman method [23]. They showed sharp diamagnetic transition at  $T_c$  and samples made in the same way had been used in previous single-crystal neutron scattering studies [5, 24]. An orientated crystal of  $3 \times 1 \times 0.5 \text{ mm}^3$  was loaded into a Paris-Edinburgh high-pressure cell together with lead powder serving as the pressure transmitting medium as well as the pressure gauge [25]. Neutron diffraction experiments were carried out using the SNAP instrument at the Spallation Neutron Source (SNS) at the Oak Ridge National Laboratory (ORNL). Two separate banks of position sensitive detectors were centered at the scattering angle  $2\theta = 48.9^\circ$  and  $90^\circ$ , respectively. Two wavelength ranges were used during the time-of-flight diffraction measurements: 1)  $0.5 \leq \lambda \leq 3.8 \text{ \AA}$  and 2)  $4.5 \leq \lambda \leq 8.3 \text{ \AA}$  to access different  $d$ -spacing ranges. The data were collected up to 9 GPa at 297 K, and 5.7 GPa at 365 K. Pressure was adjusted at constant temperature during the measurements. We label the wavevector transfer  $\mathbf{Q} = (H, K, L)$  using the tetragonal  $I4/m$  unit cell, with  $a = 8.683$  and  $c = 14.39 \text{ \AA}$  at ambient pressure [5].

Fig. 1 shows the schematic setup of the single crystal experiments. The superlattice reflections of AFM and Fe-vacancy orders are well separated from main nuclear Bragg peaks and appear at different regions of the detector banks. This is an advantage over our unpublished

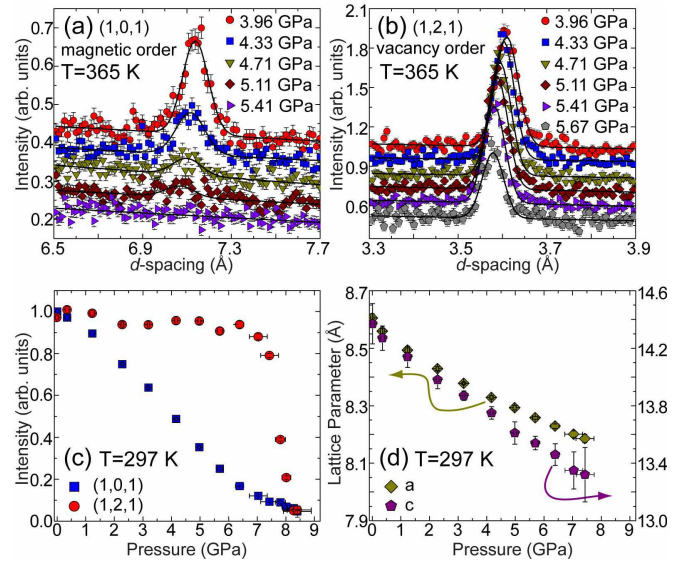


FIG. 2. (color online) (a) Magnetic (1,0,1) and (b) vacancy (1,2,1) peaks at selected pressures at 365 K. (c) Pressure dependence of the integrated intensity of the vacancy and magnetic peaks at 297 K. (d) The lattice parameters of the  $I4/m$  structure as a function of pressure at 297 K.

high-pressure powder diffraction study, where the magnetic (1,0,1) peak is close to the nuclear (0,0,2) peak. Their similar  $d$ -spacings hinder a reliable analysis of the high-pressure powder neutron diffraction data.

Fig. 2(a)-(b) show the diffraction peak profile at selected pressures for the magnetic (1,0,1) and the vacancy superlattice (1,2,1) reflections at 365 K. Both peaks are smoothly suppressed in intensity without splitting or appreciable broadening. Fitting of the integrated intensities of the peaks as a function of pressure yields critical pressure  $P_M(365\text{K}) = 5.3(2)$  GPa for the AFM order and  $P_S(365\text{K}) = 5.9(2)$  GPa for the  $\sqrt{5} \times \sqrt{5}$  Fe vacancy superstructure. Fig. 3(a)-3(b) show contour plots of the diffraction data at 365 K. Clearly the magnetic peak disappears at a lower pressure than the vacancy superlattice peak. Figs. 3(d)-(e) present contour plots for the same two Bragg peaks at 297 K. Both resolution-limited peaks indicate that the vacancy and magnetic orders remain long-ranged before their suppression by high pressure.

In Figs. 3(b) and (e), the (1,2,1) peak of the Fe vacancy order is suppressed more abruptly than the magnetic (1,0,1) peak in (a) and (d). Fig. 2(c) shows the integrated intensity of the two peaks at 297 K respectively. In contrast to the gradual suppression of the AFM order, the Fe vacancy order exhibits a precipitous drop at  $P_c \approx 8.3$  GPa. Such a behavior closely resembles the  $T$ -dependence of the two long-range orders at ambient pressure observed in previous neutron diffraction studies [4, 5]. Therefore, both at ambient and high pressures, the order parameter of the  $\sqrt{5} \times \sqrt{5}$  vacancy structure reaches the saturated value when there grows the block

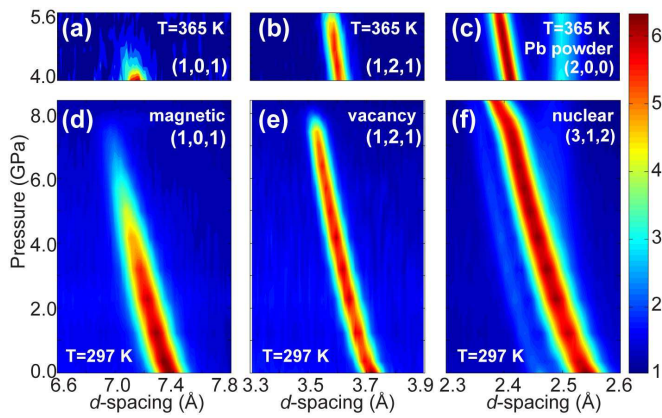


FIG. 3. (color online) Contour plots of Bragg intensity of the magnetic peak (1,0,1) at (a) 365 K and (d) 297 K; the vacancy superlattice peak (1,2,1) at (b) 365 K and (e) 297 K; (f) the main nuclear Bragg peak (3,1,2) at 297 K. (c) The (200) Bragg peak of Pb inside the pressure anvil cell at 365 K. The weak pressure-independent intensity at  $d$ -spacing 2.51 Å is the diffraction from the pressure cell.

AFM order.

Fig. 3(f) shows the nuclear (3,1,2) reflection which survives in the  $I4/mmm$  structure after the suppression of the  $\sqrt{5} \times \sqrt{5}$  superstructure under pressure. The lack of peak splitting and absence of additional reflection in the pressure tuning between the  $I4/mmm$  and  $I4/m$  structures differ markedly from what have been observed in the temperature tuning of phase-separated samples [12]. There is an inflection in the peak position at  $P_c$  in Figs. 3(f), indicating lattice parameter relaxation after the sample experiences the pressure-induced  $I4/m$  to  $I4/mmm$  structural transition. The lattice parameters  $a$  and  $c$  from least-square refinements from a number of Bragg reflections including (1,0,1), (1,2,1), (3,1,2), and (5,0,3) at 297 K are shown in Fig. 2(d) as a function of pressure. Both shrink smoothly and do not exhibit any anomalies below  $P_c$  in the vacancy ordered state. Within the Fe vacancy-ordered  $I4/m$  phase,  $(\text{Tl,Rb})_2\text{Fe}_4\text{Se}_5$  exhibits moderate anisotropic compressibility: the lattice parameter  $c$  is reduced by about 9.3% and the in-plane lattice parameter  $a$  decreases by 5% at 7.5 GPa. This contrasts with the result found in  $\text{CaFe}_2\text{As}_2$ , where the  $c$ -axis collapses with application of merely 0.4 GPa [26] and the pressure-induced structure transition destroys AFM order without introducing superconductivity [26, 27].

Sample pressure was monitored *in situ* by measuring the  $d$ -spacing of the lead (2,0,0) Bragg peak. Fig. 3(c) shows an example of its clear pressure evolution. After releasing the pressure from above  $P_c$  back to zero at 297 K, all characteristic reflections associated with the magnetic and vacancy orders in the  $I4/m$  phase reappear. However, intensity of the magnetic peak (1,0,1) is only 15 percent of the original value at ambient pressure, although intensity of the vacancy order peak (1,2,1) and

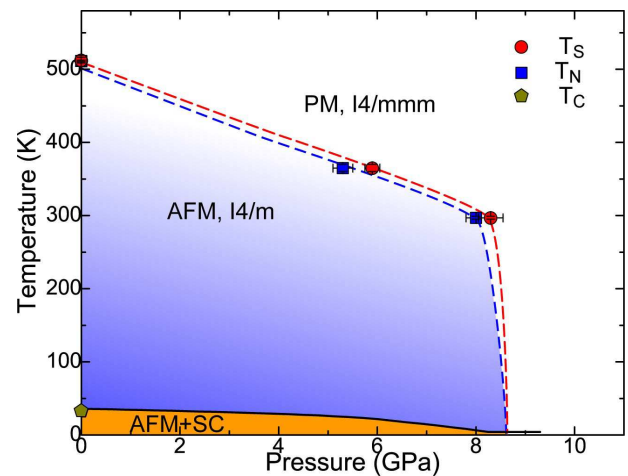


FIG. 4. (color online) Pressure-temperature phase diagram of  $(\text{Tl,Rb})_2\text{Fe}_4\text{Se}_5$ . Red circles denote the transition to the  $\text{Fe } \sqrt{5} \times \sqrt{5}$  vacancy order, and blue squares the block AFM order. Brown pentagon from magnetization measurement denotes the superconducting transition at  $P=0$ , and  $T_c$  at high pressure is adopted from [22].

the main nuclear peak (3,1,2) are fully recovered. This indicates that the  $\sqrt{5} \times \sqrt{5}$  vacancy order can sustain the pressure-cycling but the AFM order cannot recover its original fully ordered state in the constant temperature cycle.

The  $P$ - $T$  phase diagram based on neutron results is shown in Fig. 4. At ambient pressure, Fe vacancies in  $(\text{Tl,Rb})_2\text{Fe}_4\text{Se}_5$  form a highly ordered  $\sqrt{5} \times \sqrt{5}$  superlattice at  $T_S \approx 512$  K which is followed by the block AFM order at  $T_N \approx 511$  K. Both  $T_S$  and  $T_N$  are suppressed continuously by pressure, and the vacancy and AFM orders are absent at 9 GPa. The critical pressure coincides well with the pressure where the superconductivity was suppressed in the high-pressure resistivity and AC magnetic susceptibility works on  $(\text{Tl,Rb})_2\text{Fe}_4\text{Se}_5$  [22]. This phase-diagram provides direct evidence indicating an intimate connection of the superconductivity with the block AFM order developing on the iron-vacancy superlattice in the 245 superconductor. While  $T_S$  and  $T_N$  track each other (Fig. 4), interestingly the superconducting transition temperature  $T_c$  tracks the magnetic (1,0,1) Bragg intensity more closely than the superlattice (1,2,1) Bragg intensity under pressure.

Ksenofontov et al. reported that both the  $A_x\text{Fe}_2\text{Se}_2$  phase and the vacancy ordered  $I4/m$  phase survive well above  $P_c$ , and there is no structural transition up to 15.6 GPa [20]. The block AFM order only starts to slowly decrease above  $P_c$  in their high-pressure studies. However, our results clearly show that the  $\sqrt{5} \times \sqrt{5}$  Fe vacancy order and the AFM order are completely suppressed above  $P_c$ . The result for the vacancy superstructure order by Guo et al. is consistent with ours after the poor counting statistics in their high-pressure *powder* x-ray diffraction



data is taken into account [18]. Thus, there was likely either an error in the pressure calibration or too large a pressure gradient in the work of Ksenofontov *et al.* Accordingly, their conclusion that the  $A_x\text{Fe}_2\text{Se}_2$  phase survives above  $P_c$  may also be in doubt, although nobody has been able to detect the weak signal from the  $A_x\text{Fe}_2\text{Se}_2$  phase in any high-pressure diffraction experiment so far.

The importance of the Fe vacancy order has also been demonstrated by transport property. The metal-like resistivity behavior is a precursor to superconductivity and corresponds to a highly ordered  $\sqrt{5} \times \sqrt{5}$  Fe vacancy superlattice [4, 8]. The nonsuperconducting samples, on the other hand, contain imperfect Fe vacancy order which introduces substantial site disorder. The similar property has been shown in the  $\text{Fe}_{1+x}(\text{Se},\text{Te})$  superconductors for which disordered spin scattering induced by the interstitial excess Fe is responsible for the metal-semiconductor crossover [28]. The scanning tunneling spectroscopy study on  $\text{KFe}_2\text{Se}_2$  films, in which random Fe vacancies serve as spin carrying scatterers, also show the same microscopic behavior that is destructive to the local superconducting gap [11].

Additionally, the  $\sqrt{5} \times \sqrt{5}$  vacancy order with its associated AFM order is substantially more stable with the magnetostructural energy gain through the formation of the Fe tetramers [29, 30]. It is thus conceivable that the few percent Fe at the minority Fe1 site in the average  $I4/m$  structure of the 245 superconductors [4, 6, 12], instead of being randomly distributed, aggregates to form nanoscale phase separation in order to save energy in breaking up the tetramers. Close interaction between the superconducting and AFM order parameters is therefore expected. When the excess Fe at the Fe1 sites aggregate on the  $\sqrt{5} \times \sqrt{5}$  superlattice of fully ordered Fe2 sites, site disorder is minimized and so is the pair-breaking electron scattering. The local composition inside the aggregation is  $A_{0.8}\text{Fe}_2\text{Se}_2$  and outside it  $A_{0.8}\text{Fe}_{1.6}\text{Se}_2$ , which average to a  $A_{0.8}\text{Fe}_{1.6+\delta}\text{Se}_2$  sample composition. When the highly ordered  $I4/m$  phase is suppressed at high pressure for the superconducting samples or is upset in nonsuperconducting samples, the energetics driving the formation of phase segregation is lost, so is the superconductivity.

In summary, we have performed high-pressure single-crystal neutron diffraction study on magnetic and structural transitions in  $(\text{Tl},\text{Rl})_2\text{Fe}_4\text{Se}_5$  superconductor. We found both the  $\sqrt{5} \times \sqrt{5}$  Fe vacancy order and the block AFM order are suppressed at  $P_c = 8.3$  GPa, where superconductivity also diminishes. As in previous temperature dependent studies, the AFM order is also instrumental in the stability of the Fe vacancy order under pressure. Our

results demonstrate that the highly ordered  $\sqrt{5} \times \sqrt{5}$  vacancy order and associated block AFM order are crucial ingredients in the realization of 245 superconductors.

The works at RUC and ZU were supported by the National Basic Research Program of China Grant Nos. 2012CB921700, 2011CBA00112, 2011CBA00103 and 2012CB821404, by the National Science Foundation of China Grant Nos. 11034012, 11190024, 11374261 and 11204059, and by Zhejiang Provincial Natural Science Foundation Grant No. LQ12A04007. Research at ORNL's SNS was sponsored by the Scientific User Facilities Division, Office of Basic Energy Sciences, U.S. DOE.

---

\* wbao@ruc.edu.cn

- [1] J. Guo *et al.*, Phys. Rev. B **82**, 180520(R) (2010).
- [2] E. Dagotto, Rev. Mod. Phys. **85**, 849 (2012).
- [3] Z. Shermadini *et al.*, Phys. Rev. Lett. **106**, 117602 (2011).
- [4] W. Bao *et al.*, Chin. Phys. Lett. **28**, 086104 (2011).
- [5] F. Ye *et al.*, Phys. Rev. Lett. **107**, 137003 (2011).
- [6] P. Zavalij *et al.*, Phys. Rev. B **83**, 132509 (2011).
- [7] J. Bacsá *et al.*, Chem. Sci. **2**, 1054 (2011).
- [8] W. Bao *et al.*, Chin. Phys. Lett. **30**, 027402 (2013).
- [9] Z. Wang *et al.*, Phys. Rev. B **83**, 140505 (2011).
- [10] J. Zhao, H. Cao, E. Bourret-Courchesne, D.-H. Lee, and R. J. Birgeneau, Phys. Rev. Lett. **109**, 267003 (2012).
- [11] W. Li *et al.*, Nature Phys. **8**, 126 (2011).
- [12] D. P. Shoemaker *et al.*, Phys. Rev. B **86**, 184511 (2012).
- [13] Y. Texier *et al.*, Phys. Rev. Lett. **108**, 237002 (2012).
- [14] S. Weyeneth *et al.*, Phys. Rev. B **86**, 134530 (2012).
- [15] A. Ricci *et al.*, Phys. Rev. B **84**, 060511(R) (2011).
- [16] Y. Liu, Q. Xing, K. W. Dennis, R. W. McCallum, and T. A. Lograsso, Phys. Rev. B **86**, 144507 (2012).
- [17] A. Charnukha *et al.*, Phys. Rev. Lett. **109**, 017003 (2012).
- [18] J. Guo *et al.*, Phys. Rev. Lett. **108**, 197001 (2012).
- [19] M. Gooch *et al.*, Phys. Rev. B **84**, 184517 (2011).
- [20] V. Ksenofontov *et al.*, Phys. Rev. B **85**, 214519 (2012).
- [21] G. Seyfarth *et al.*, Solid State Communications **151**, 747 (2011).
- [22] L. L. Sun *et al.*, Nature **483**, 67 (2012).
- [23] H. Wang *et al.*, Europhys. Lett. **93**, 47004 (2011).
- [24] S. Chi *et al.*, Phys. Rev. B **87**, 100501(R) (2013).
- [25] O. Schulte and W. B. Holzapfel, Phys. Rev. B **52**, 12636 (1995).
- [26] A. Goldman *et al.*, Phys. Rev. B **79**, 024513 (2009).
- [27] W. Yu *et al.*, Phys. Rev. B **79**, 020511(R) (2009).
- [28] T. Liu *et al.*, Nature Mat. **9**, 716 (2010).
- [29] C. Cao and J. Dai, Phys. Rev. Lett. **107**, 056401 (2011).
- [30] X.-W. Yan, M. Gao, Z.-Y. Lu, and T. Xiang, Phys. Rev. B **83**, 233205 (2011).